JPRS-JST-93-005
1 February 1993

DISTRIBUTION STATEMENT A
Approved for public release;
Distribution Unlimited

JPRS Report

Science & Technology

Japan
Developments in Inorganic Advanced Materials

DTIC QUALITY INSPECTED 2

19980506 080

REPRODUCED BY
U.S. DEPARTMENT OF COMMERCE
NATIONAL TECHNICAL INFORMATION SERVICE
SPRINGFIELD, VA 22161

Science & Technology

Japan

Developments in Inorganic Advanced Materials

JPRS-JST-93-005 *1 February 1993*

CONTENTS

[Selected papers from Report on Results of Grant-in-Aid Science and Technology Research FY91 (Research on Priority Areas, No 1)]

Improvement and Evaluation of Inorganic Advanced Materials Strength

Table of Contents

93FE0024A Tokyo HEISEI 3-NENDO KAGAKU KENKYUHI HOJOKIN in Japanese Mar 92 pp i-v

[Text]

A02 "Structural Control, Plastic Processability, Surface Processability and Tribology of Inorganic Advanced Materials"

A03 "Mechanics and Properties of Boundary Behaviors of Joints and Advanced Composite Materials"

Preface

93FE0024B Tokyo HEISEI 3-NENDO KAGAKU KENKYUHI HOJOKIN in Japanese Mar 92 p 1

[Text]

Priority Area Research Project: "Improvement and Evaluation of Strength of Inorganic Advanced Materials"
Summary of FY91 Project Achievements
Project Representative: Takeo Yokobori, Professor
Department of Science and Engineering, Teikyo University

Para. 1. Foreword

Given below is a summary of the project systematization and achievements in FY91, including the proposal of new concepts and criteria, their verifications, surveys and analyses. The summarized project systematization in terms of project direction determined by surveys and analyses carried out in this project and other related projects is presented in Sections Para. 2 through Para. 7. The summary of proposed new concepts and their verifications is given in Para. 8 through Para. 17. Project achievements involve many diverse fields, so that details should be found in each project report.

Para. 2. Objective of The Priority Area Research Project: "Improvement and Evaluation of Strength of Inorganic Advanced Materials"

Main efforts in the research concerning material strength, mechanical properties and fracture (to be called simply 'material strength' hereafter) were previously placed on the evaluation merely to maintain and improve reliability of materials as structures. In other words, the fact that the mechanical engineering field was the leading force behind the material strength research appears to confirm the above-mentioned placement of main efforts. For example, the majority of research projects that received an allotment of science research fund from the Ministry of Education was concerned with mechanical engineering. In addition, these projects themselves were intended mostly for material reliability improvement, rather than for material development. However, material strength research is indispensable not only for reliability evaluation but also for material structure design and processing method development. Because, through material strength research, new advanced materials with unquestionably higher strength and the fantastic capability of being fabricated into required shapes and forms must be created and developed, and the performance of traditional materials can be improved as well.

Thus, for the past 10 years, the urgency for the research field which integrates material science theory, material structural science and bulk material dynamics on material strength has been recognized based on this point of view, and researchers have also shown increasing interest in the field. This constitutes the objective of this area research project.

Development of New Methods and Their Mechanical Behavior

93FE0111A Tokyo HEISEI SAN NENDO KAGAKU KENKYUHI HOJOKIN in Japanese Mar 92 pp 19-20

[Article by Teruo Kishi, Advanced Science and Technology Research Center, Tokyo University]

[Text]

"Development of New Techniques and Clarification of Mechanical Behavior by These Techniques"

A01 Section pursued the development of new measurement and evaluation techniques and their applications for inorganic advanced materials, and achieved the following.

(1) Composite formation is an effective technique to overcome brittleness of ceramics. The hot press method was used to prepare a composite material consisting of the glass matrix and SiC long fibers. First, a single fiber test method was established, and the method was used successfully to quantitatively evaluate interfacial mechanical property values, including interfacial shear stress, friction coefficient and clamping stress values. With these values, the crack propagation resistance values were calculated for uni-directionally fiber-reinforced materials. These values agreed well with experimental values. Furthermore, test specimens were prepared under different process conditions, and tests were carried out with a varying loading rate, to seek interfacial property parameters. Thus, in conclusion, the interfacial property evaluation method for composite materials was established. (Group led by Teruo Kishi)

(2) The controlled breakage forming method, a new method for preparing composite wires, was developed, and an α-Al_2O_3 composite wire was prepared by the new method (Group led by Tatsuhiko Aizawa). In addition, the sintering characteristics of micronized Si_3N_4 were examined (Group led by Genji Jimbo), and the basic principles for powder sintering were outlined.

(3) Long fibers, micro-composite materials in which various second-phase grains were dispersed, nano-composite materials and hybrid composite materials were prepared; and the principles for developing ceramic-based nano-composite materials with excellent strength and toughness were clarified (Group led by Koichi Niihara).

(4) The relationship of strength of SiC whisker-dispersed Si_3N_4 ceramics to the addition of sintering aid (Group led by Koji Hayashi), and the material design for improving composite toughness of grain-dispersed ceramics (Group led by Noboru Miyata) were outlined.

(5) In order to develop techniques for evaluating mechanical properties of inorganic advanced materials, the relationships among surface conditions, internal flaws and strength were studied (Group led by Ichiro Maekawa); the relationship of ceramics fatigue to stress

corrosion was clarified (Group led by Hideo Kobayashi); and attempts were made to develop an evaluation method and its applications for thermal shock fracture toughness (Group led by Hiroomi Homma), and shock characteristics and thermal shock characteristics (Group led by Hiroo Takeda).

(6) Fracture patterns were studied by simulation (Group led by Shuji Shimamura); Monte Carlo simulation for strength distribution was studied (Group led by Michina Tanaka); and a reliability evaluation method was studied by correlation of limiting physical properties (Group led by Hiroaki Yanagida).

(7) A technique for obtaining high-temperature anisotropic elastic moduli via thermal shock was established (Group led by Masaru Sakata); and it was clarified that grain boundary slippage could be detected by high-temperature pseudo-elasticity measurement (Group led by Koichi Tanaka).

(8) In order to develop new non-destructive techniques for advanced materials, attempts were made to detect microscopic flaws by the AE method (Group led by Yasuhiko Mori), to derive microcrack formation stresses by the AE method (Group led by Shuichi Wakayama), and to show the effectiveness of an ultrasonic damage evaluation technique (Group led by Hiroyuki Okamura).

In conclusion, attempts were made to control primarily ceramic powder materials; nano-, micro- and long fiber composite materials were prepared; proposals were made and applications were tested for new mechanical property evaluation techniques; and detection of microscopic flaws were studied with non-destructive test methods. Thus, significant achievements were made toward the establishment of new measurement evaluation techniques and the development of highly functional ceramic-based composite materials.

Evaluation of Fatigue, Stress Corrosion Crack Properties of Ceramics

93FE0111B Tokyo HEISEI SAN NENDO KAGAKU KENKYUHI HOJOKIN in Japanese Mar 92 pp 51-57

[Article by Hideo Kobayashi, Department of Engineering, Tokyo Institute of Technology]

[Text]

1. Introduction

Destructive mechanical techniques are useful for evaluating strength of structural ceramics, because they are manufactured with inherent flaws, and it is considered desirable to accumulate basic data concerning plane strain fracture toughness values. However, since it is difficult to introduce fatigue precracks into a ceramic material, one cannot use its through-drilled compact test specimens which are in general use for destructive mechanical tests. Therefore, several alternate methods have been proposed, and they include the single edge precracked beam (SEPB) method, the chevron notched test specimen method, and the indenter forcing (IF) method. However, side effects, including those by crack progression due to stress corrosion cracking in the middle of a loading process, cannot be ignored at times when these tests are performed. In order to analyze these effects, the evaluation of stress corrosion crack characteristics is desired from the standpoint of fracture toughness evaluation. Furthermore, attention has recently been focused on the relationship, i.e., the mutual actions between fatigues due to stress corrosion cracks and repeated loading and stress corrosion cracks themselves, from the standpoint of guaranteeing structural safety of materials through proof tests by actual testers. Thus, the objective of this project was to evaluate stress corrosion cracks and fatigue characteristics of mechanical-structural ceramic materials. Using a technique for generating the progression of fatigue cracks from compression damages by repetitive loading, Su_3N_4 and SiC were tested, and their behavior was analyzed on the basis of fracture dynamics.

2. Materials and Experimental Methods

Materials tested were normal-pressure silicon nitride and silicon carbide. Their mechanical properties are presented in Tables 1 and 2.

Table 1. Mechanical Properties of Si_3N_4

Young's modulus	Flexural strength	Compressive strength
274 GPa	882 MPa	3,920 MPa

Table 2. Mechanical Properties of SiC

Young's modulus	Flexural strength	Compressive strength
402 MPa	539 MPa	—

For tests, 1/2-inch compact specimens (W = 25.5 mm and B = 10 mm for Si_3N_4, and B = 8.5 mm for SiC) were used. A front-edge radius of curvature, ρ = 0.5 mm, (length, a_0 = 15.3 mm) was used for notching each test specimen. The sides of the test specimen were treated with gold sputtering to make it easy to measure cracks.

All tests were carried out in the atmosphere at room temperature, using a 19.6 kN-capacity electro-hydraulic servo tester. A crosshead displacement speed of 2.5 x 10^{-3} m/sec was used for fracture toughness tests. Fracture tests were carried out with a constant stress ratio, R = 0.1, 0.5 and 0.8, and with the stress expansion constant range, ΔK, on a steady decrease and increase. However, due to the difficulty in controlling a load for the tester, the load was step-wise decreased for each displacement, Δa, of 0.1 mm, in accordance with E647 of ASTM. Furthermore, a strain gauge was attached on the backside of each test specimen in order to be able to measure crack opening stress expansion constant K_{op}. A metal microscope (magnification of 220 x) was used to measure crack lengths. A weight was used to subject a test specimen to an long-hour dead weight for the stress

corrosion crack test. Incidentally, the aforementioned tester was used for short-hour loading (less than 1.0×10^3 sec). The same technique as the one used for the fatigue test was used to measure crack lengths.

The technique of introducing a fatigue precrack, which had been reported by Suresh et al.,[1] was applied for the compact test specimens. After a compression break was introduced at the front edge of the notch, a test specimen is subjected to a repetitive tensile load. The test specimen was clamped by metallic jigs whose respective top and bottom planes were fixed in parallel to each other, and a specified load was added to the test specimen and held for 3 seconds before removing the load. Again, a strain gauge was attached to the backside of the test specimen to be sure that no tensile load due to bending be generated during the compression stage. A compression break of approximately 100 μm was created at the notch bottom of silicon nitride test specimens at approximately -130 kN. A similar break was also produced in silicon carbide at approximately 75 kN. Subsequently, the test specimens were subjected to repetitive tensile loading with a stress ratio, R = 0.1, and a maximum stress expansion constant, K_{max}, which was equivalent to approximately 90% of the fracture toughness values, to introduce an approximately 1-mm-long fatigue precrack to each test specimen.

3. Results and Discussion

Results of actual measurements are plotted in Figure 1 for the relationship between the fatigue crack progression speed, da/dN, and the stress expansion constant range, ΔK, for silicon nitride. With the increase in the stress ratio, R, for the repetitive loading from 0.1 (marked with open circles) to 0.5 (marked with open triangles) and to 0.8 (marked with open squares), the fatigue crack progression speed increases. In addition, the solid circle marks in the graph indicate data obtained when the length of the introduced precrack, Δa, was smaller than the notch radius, ρ. Compared with data obtained when $\Delta a \geq \rho$, the solid-circle data are located on the deceleration side.

Shown in Figure 2 are the results of measurements of the ratios of the crack-closing stress expansion constant and the maximum expansion constant, K_{op}/K_{max}, for R = 0.1 and 0.5.

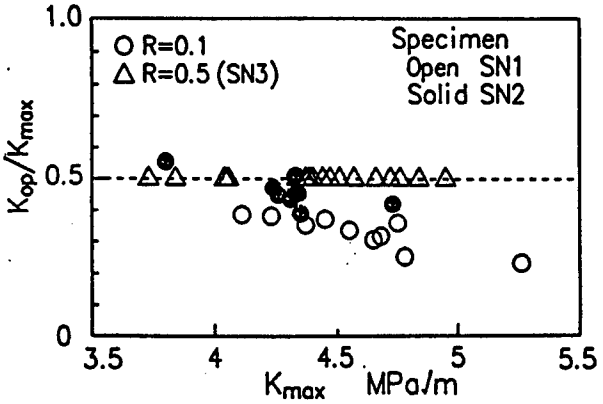

Figure 2. Relationship of K_{op}/K_{max} to K_{max} for Si_3N_4

In the case of R = 0.1, K_{op}/K_{max} increases monotonically with a decrease in K_{max}, with the crack closing phenomenon being clearly recognized, although there is a difference between the two different test specimens (SN1 with open circles, and SN2 with solid circles). In the case of R = 0.5, crack closure is not recognized with a decrease in K_{max}. Figure 3 shows the relationship of da/dN to the effective stress expansion constant, ΔK_{eff} (= K_{max} - K_{op}), with the use of experimental values for the crack closure. In this graph, the data for R = 0.1 and R = 0.5 are comparatively close together, while the data for R= 0.8 are completely off. Also, data appear scattered for different test specimens. The same fatigue crack progression speed is further expressed in terms of the maximum stress expansion constant, K_{max}, for the repetitive loading in Figure 4. It is clear from this graph that the factor governing the fatigue crack progression speed is K_{max}. A similar graph for silicon carbide is shown in Figure 5. Compared with silicon nitride, the fracture toughness value is lower and the load stress expansion constant range for fatigue crack progression is narrower for silicon carbide.

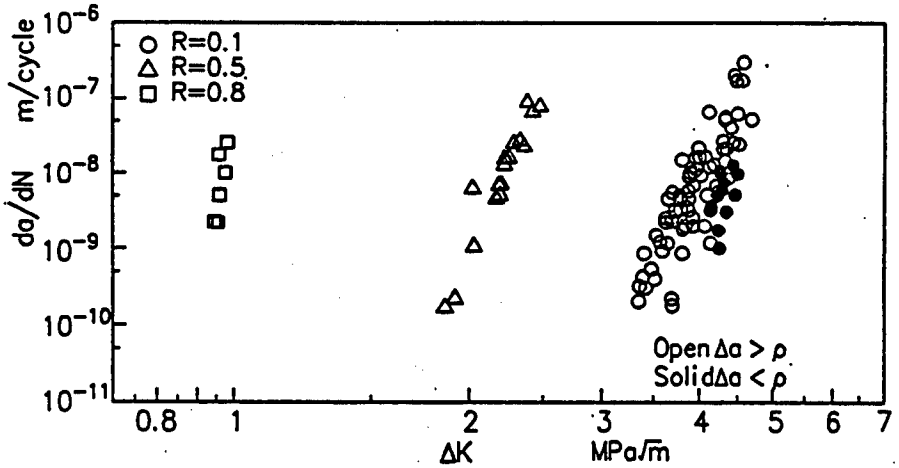

Figure 1. Relationship da/dN to ΔK for Si_3N_4

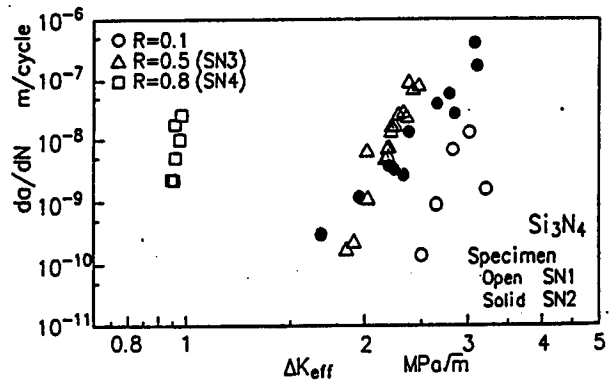

Figure 3. Relationship of da/dN to ΔK_{eff} for Si_3N_4

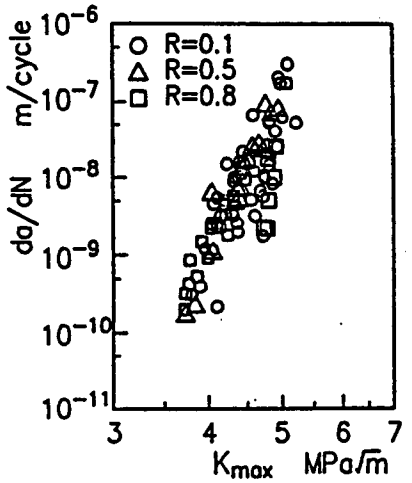

Figure 4. Relationship of da/dN to K_{max} for Si_3N_4

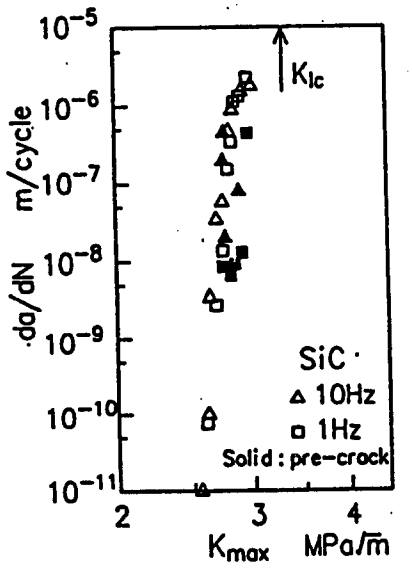

Figure 5. Relationship of da/dN to K_{max} for SiC

Actually measured stress corrosion crack progression speed, da/dt, for silicon nitride are graphically presented in Figure 6. The lower limiting value, K_{ISCC}, for stress corrosion cracks is 4.63MPa(m)$^{1/2}$, which is approximately 87% of the fracture toughness value, K_{IC} (= 5.32 MPa(m)$^{1/2}$), for silicon nitride. In order to compare the stress corrosion crack progression with the fatigue crack progression, an assumption was made that the fatigue crack progression would be caused only by stress corrosion cracking, and this assumption was tested for its validity by comparing predicted values for the fatigue crack progression speed under repetitive loading with actually measured values. The crack progression speed for stress corrosion cracking is expressed by Equation (1).

$$da/dN = 2.16 \times 10^{-77} K_{max}^{100} \qquad (1)$$

From Equation (1), the magnitude of crack progression, Δa, within the time period, Δt, is as follows.

$$\Delta a = 2.16 \times 10^{-77} K(t)^{100} \Delta t$$

$$K(t) = K_m + \Delta K/2 \sin(2\pi ft) \qquad (2)$$

where $K_m = (K_{max} + K_{min})/2$ and f is the frequency of repetitive loading. By integrating Equation (2) for one cycle, the crack progression magnitude, da/dN, per cycle of repetitive loading can be obtained.

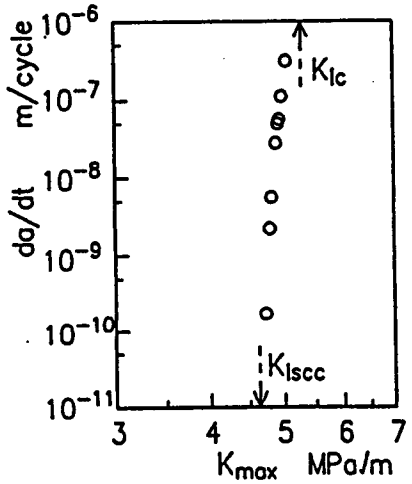

Figure 6. Relationship of da/dt to K_{max} for Si_3N_4

The cases of the frequency being 10 Hz and 1 Hz were analyzed, and the results are shown in Figure 7. In this graph, the solid line denotes the analytical results for 10 Hz, and the dotted line denotes those for 1Hz. On the higher K_{max} side, the experimental values and the analytical values are closer to each other, indicating that the effects of stress corrosion cracking are predominant. On the other hand, on the lower K_{max} side, the analytical values are situated on the deceleration side, indicating a danger sign, if stress corrosion cracking is assumed to be the only factor. In particular, the experimental values obtained under the repetitive loading conditions suggest

crack progression even if K_{max} is less than K_{ISCC}. Thus, the dependence of the fatigue crack progression speed on K_{max} cannot be explained only in terms of stress corrosion cracking.

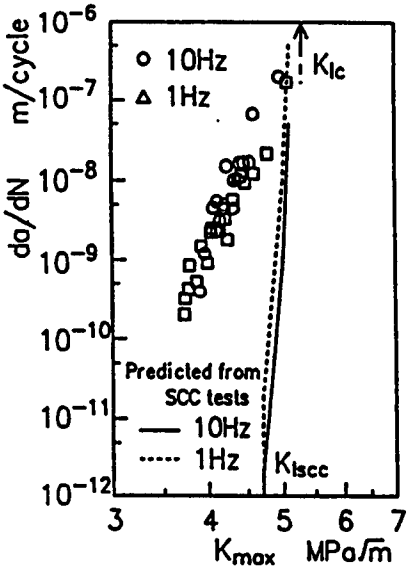

Figure 7. Relationship of da/dt to K_{max} for Si_3N_4

4. Conclusion

The fatigue crack progression characteristics and the stress corrosion cracking characteristics of structural ceramics were examined with experiments. Results can be summarized as follows.

(1) The governing factor for the fatigue crack progression speed is the load's maximum stress expansion constant.

(2) Fatigue crack closure accompanies crack progression, although there is no effect upon the crack progression speed.

(3) The fatigue crack progression speed is influenced by stress corrosion cracking in a region above the lower limit stress expansion constant for stress corrosion cracking, although the K_{max} dependence of the fatigue crack progression speed cannot be explained in terms of only stress corrosion cracking.

Reference

1. S. Suresh, "Fatigue 90", Nov. 1989.

Oral Presentation

1. Haruo Nakamura, Hideo Kobayashi, Masafumi Sensaki and Nagatoshi Okabe; "Examination of Simple Evaluation Techniques for Fracture Toughness of Silicon Nitride," Lecture and Dissertation Collection on Fracture and New Technologies, Material Dynamics Symposium, pp 900-950, Japan Society of Mechanical Engineers (1990) 377/388.

Development of Ceramic Nano Composites

93FE0111C Tokyo HEISEI SEN NENDO KAGAKU KENKYUHI HOJOKIN in Japanese Mar 92 pp 83-87

[Article by Koichi Niihara and Atsushi Nakahira, Industrial Science Research Institute, Osaka University]

[Text]

1. Introduction

Studies were conducted to introduce new material design into the field of ceramics on the basis of a classification of ceramics into monolithic and composite materials, with the latter further divided into micro-composite, nano-composite and micro/nano-hybrid materials. As a result of these studies, it was discovered that mechanical properties of ceramics were drastically improved through the formation of trans-granular nano-composites by dispersing nano-size second-phase particles either within crystal grains or crystal interstices of the matrix. In addition, these nano-composites were successfully converted, through micro/nano-hybridization with long-fiber reinforcement, into new materials with super strength and toughness up to 1,500°C. These experiments are outlined below.

2. Preparation of Nano-Composites and Long-Fiber-Reinforced Nano-Composites

Nano-composites were successfully prepared using an ordinary sintering method for Al_2O_3/SiC, Al_2O_3/Si_3N_4, Al_2O_3/TiC, MgO/SiC, mullite/SiC, SiC/amorphous SiC, Si_3N_4/SiC and B_4C/SiC. Of these nano-composites, Si_3N_4/SiC could also be prepared by sintering, in a liquid phase, Si-C-N amorphous composite powder made by the CVD method, with the addition of Al_2O_3 and Y_2O_3 as sintering aids, at a temperature between 1,600°C and 1,800°C. In this preparation process, it is conjectured that nano-size SiC particles play a role of growth nuclei for β-Si_3N_4 to re-precipitate and sinter, after α-Si_3N_4, formed from the amorphous Si-C-N powder, has been dissolved in the liquid phase. All other nano-composites than Si_3N_4/SiC were prepared by sintering in a solid phase. The following conditions were found to be important for the formation of these nano-composites: (1) two raw material powders should be selected to have their average particle diameters be less than 0.4 μm; (2) the two powders should be mixed uniformly; and (3) sintering conditions should be such that grains of the dispersed phase will not grow, while grains of the matrix grow fast.

The micro/nano-hybrid materials, i.e., long carbon fiber-reinforced Sialon/SiC nano-composites, were prepared as follows to realize super strength and toughness. Raw materials, including Al_2O_3, Si_3N_4, SiC powder, polysilazane which becomes Si_3N_4 when heated to a high temperature, and long carbon fibers, were molded with toluene as a binder, and the molded material was reaction-sintered under high pressure.

3. Improvement of Mechanical Properties Through Formation of Nano-Composite

Improvements in mechanical properties for the composite systems of Al_2O_3/SiC, Al_2O_3/Si_3N_4, MgO/SiC, Si_3N_4/SiC and mullite/SiC are presented in Table 1. The fracture strength of the Al_2O_3/SiC nano-composite system jumps from approximately 350 MPa to approximately 1,500 MPa by dispersing 5-volume percent of SiC particles in crystal grains of the matrix. Furthermore, Table 1 also indicates marked strength increases for the Al_2O_3/Si_3N_4 nano-composite system (from approximately 350 MPa to 850 MPa) and for the MgO/SiC nano-composite system (from approximately 350 MPa to 700 MPa). Fracture toughness values also increased by approximately 50% for both Al_2O_3/SiC and Al_2O_3/Si_3N_4 systems, and the same roughly quadrupled for the MgO/SiC. In addition, abnormal improvements of approximately 400°C and approximately 700°C were observed for the maximum temperatures (the transition temperatures from brittle fracture to ductile fracture) at which the Al_2O_3-based composites and the MgO-based composites, respectively, could still be used under a high load.

Table 1. Improvements in Mechanical Properties of Ceramics Through Formation of Nano-Composite

Composite	Toughness ($MPam^{1/2}$)	Strength (MPa)	Maximum Use Temperature (°C)
Al_2O_3/SiC	3.5 → 4.8	350 → 1,520	800 → 1,200
Al_2O_3/Si_3N_4	3.5 → 4.7	350 → 850	800 → 1,300
MgO/SiC	1.2 → 4.5	340 → 700	600 → 1,400
Mullite/SiC	1.2 → 3.5	150 → 700	700 → 1,200
Si_3N_4/SiC	4.5 → 7.5	850 → 1,550	1,200 → 1,400

The size and shape of the Si_3N_4 grains in the Si_3N_4/SiC nano-composite system was found to be markedly influenced by dispersion of the nano-particles of SiC in the Si_3N_4 grains. When the dispersed amount of the nano-grains of SiC was less than approximately 25 volume percent, the growth of uniformly rod-shaped Si_3N_4 grains was promoted, and because of this growth, both fracture toughness and fracture strength values increased from 4.5 to approximately 7.5 $MPam^{1/2}$ and from 850 to 1,550 MPa, respectively. The fracture strength of Si_3N_4 ceramics has been known to deteriorate at temperatures higher than 1,200°C, because of the softening of the SiC-Si_3N_4 interfacial phase in the low-melting impurity, which is formed from a sintering aid and SiO_2, present on the surface of Si_3N_4, in the grain boundaries. However, the Si_3N_4/SiC nano-composite was able to maintain its strength of over 1,000 MPa at 1,400°C, because its grain boundaries were strengthened by the direct bonding between dispersed SiC and Si_3N_4 without the impurity phase between them.

4. Micro/Nano-Hybrid Materials

Although the mechanical properties of various ceramics were found to be drastically improvable through nano-composite formation, the fracture toughness values of the nano-composites were not yet sufficiently high, when compared with metallic materials. However, as clearly shown in Table 2, the data for the long carbon fiber-reinforced sialon/SiC nano-composite suggest that the fracture toughness problem can be solved through reinforcement of a nano-composite with long fibers. The strength and toughness values attained by this particular nano-composite exceed those for the currently industrially widely used super-hard material (WC/Co-based cermet). Incidentally, no report has been published concerning development of a material whose mechanical properties do not only deteriorate, but rather improve, as the temperature is increased to above 1,300°C.

Table 2. Mechanical Properties of Carbon Fiber-Reinforced Sialon/SiC Nano-Composite

Composite Material	Strength (MPa)			Toughness ($MPam^{1/2}$)	
	RT	1.300°C	1,500°C	RT	1,300°C
Long Fiber-Reinforced Sialon	314			9.5	
Long Fiber-Reinforced Sialon/SiC Nano-Composite	705	1,075	790	25.0	22.0

5. Conclusion

It was clarified that various properties of ceramic structural materials could be drastically improved through nano-composite formation by dispersing a nano-size second phase in grain boundary region or in grains themselves of the matrix. It was also found that ceramic materials that could maintain sufficient toughness to high temperatures to withstand most severe conditions could be developed by hybridizing a micro-composite and a nano-composite. In order to achieve the hybridization, it is possible to reinforce a nano-composite with plate-like grains, whiskers or long fibers. However, the experimental results indicate that the long-fiber reinforcement appears most promising. Thus, long fiber-reinforced nano-composites are predicted to be ultimate ceramic structural materials.

6. References

1. Koichi Niihara: "Design of Highly Tough Ceramics," Ceramics 26 (1991) 457-63.

2. Koichi Niihara: "Nano-Composite Ceramics," Ceramics 26 (1991) 1113-1114.

3. K. Izaki, A. Nakahira and K. Niihara: "Oxidation Resistance of Si_3N_4-32-vol-percent SiC Nanocomposites," J. Japan Soc. Powder and Powder Metallurgy, 38, (1991) 357-360.

4. K. Niihara and A. Nakahira: "Particulate Strengthened Oxide Ceramics -Nanocomposites- ," Advanced structural Inorganic Composites, Ed. P. Vincenzini, Elsevier Sci. Pub., (1991) 637-643.

5. K. Niihara: "New design Concept of Structural Ceramics -Nanocomposites-," J. Ceram. Soc. Japan, 99, (1991) 914-922.

6. A. Sawaguchi, K. Toda and K. Niihara: "Mechanical and Electrical Properties of Silicon Nitride-Silicon Carbide Nanocomposite Material," J. Amer. Ceram. Soc. 74, (1991) 1142-1144.

7. A. Sawaguchi, K. Toda and K. Niihara: "Mechanical and Electrical Properties of Al_2O_3/SiC Nanocomposites," J. Ceram. Soc. Japan (Int. Ed.), 99 (1991) 510-513.

8. M. Iwata, A. Nakahira, H. Inada and K. Niihara: "Ceramic Composites With Hybrid Matrix Via Polymer Pyrolysis," Proc. 1st Int. Symp. Sci. Eng. Ceram., The Ceramic Society of Japan (1991) 387-391.

9. T. Rouxel, F. Wakai, K. Izaki and K. Niihara: "Super-Plasticity of Si_3N_4/SiC Composites," Proc. 1st Int. Symp. Sci. of Eng. Ceram., The Ceramic Society of Japan (1991) 437-442.

10. E. Yasuda, Q. Bao, Y. Tanabe and K. Niihara: "High Temperature Creep of SiC/MgO Nanocomposite," Proc. 1st Int. Symp. Sci. of Eng. Ceram., The Ceramic Society of Japan (1991) 431-436.

11. G. Sasaki, H. Nakase, K. Suganuma and K. Niihara: "Observation of Fracture Path of SiC Particle Dispersed Si_3N_4 Composites," Proc. 1st Int. Symp. Sci. of Eng. Ceram., The Ceramic Society of Japan (1991) 291-296.

12. K. Izaki, A. Nakahira and K. Niihara: "Si_3N_4/SiC Nanocomposite From Amorphous Si-C-N Powder Precursor," Proc. 1st Int. Symp. Sci. of Eng. Ceram., The Ceramic Society of Japan (1991) 443-448.

13. T. Tanimoto, K. Suganuma and K. Niihara: "Mechanical Properties and Nanostructure of Machineable SiC." Proc. 1st Int. Symp. Sci. of Eng. Ceram., The Ceramic Society of Japan (1991) 419-424.

14. K. Niihara and A. Nakahira: "Structural Ceramic Nanocomposites," Ceramics: Toward the 21st Century, The Ceramic Society of Japan (1991) 404-417.

Composition Control and Processability and Tribology of IAM

93FE0111D Tokyo HEISEI SAN NENDO KAGAKU KENKYUHI HOJOKIN in Japanese Mar 92 pp 163-164

[Article by Yuzo Nishikawa, Department of Engineering, Kyoto Institute of Technology]

[Text]

Summary of A02 Section Research Project "Composition Control of Inorganic Advanced Materials and Their Plastic Processability, Surface Processability and Tribology"

This Research Section was organized for the purpose of developing new inorganic advanced materials, including engineering ceramics, equipped with optimal properties necessary for their application in actual devices, and of improving their mechanical processability. Given below is the summary of research achievements for FY91.

A study was conducted to clarify the mechanism of ZrO_2-Al_2O_3-based ceramics to manifest a strength of 3,000 MPa. It was concluded that the mechanism resulted from a combination of a number of conditions including residual stress in a sintered material, deformation due to the rearrangement of the ZrO_2 part, and mutual diffusion between ZrO_2 and Al_2O_3 (Nishikawa Group). It was found that the creep speeds of 3 to 10% ZrO_2-dispersed MgO ceramic materials were governed by the diffusion rate of Mg^{2+} ion, and that the strain rates of these ceramic materials at 1,400°C were extremely fast at 1×10^{-1} h^{-1} (Ikuma Group). It was confirmed that the growth of MgO grains in the 10% ZrO_2-MgO ceramic material was suppressed, and, at the same time, the grains manifested super-plastic behavior (Nishikawa Group). Furthermore, it was also discovered that the creep speed of MgO-based ceramics could be suppressed and accelerated by the dispersion of SiC and Y_2O_3, respectively (Yasuda Group).

Through thermomechanical treatment, an ($\alpha + \gamma$) microfine equi-axed grain structure was obtained with a Ti-Al-based alloy, and this material manifested superplasticity as large as several 100% (Tsujimoto Group).

The relationship of abrasive friction of Pt and Au against oxide ceramics to the surrounding atmosphere was studied, and super-low friction was observed particularly between Pt and Al_2O_3 (Hiratsuka Group).

Higher wear resistance shown by oxide ceramics than by non-oxide ceramics was examined in terms of the amount of oxygen present in the oxides (Mishina Group). Water and many organic compounds were found to be adsorbed on newly wear-created surfaces of ceramics (Mori Group).

An evaluation technique was established for brittleness, the cause for difficulty in machining ceramic materials,

by using an energy theory for the examination of non-linear surface deformation (Sakarai Group). Residual stresses for various phases in ZrO_2-Al_2O_3 composites, WC-Co and SiC-reinforced Al alloys were successfully evaluated (Tanaka Group).

Research concerning plasticity and plastic processing received priority among publicly solicited projects.

The activities in this area included the improvement of plastic processing of TiAl intermetallic compounds by structural control (Fukutomi Group); the production process development and ductility improvement for B2-type intermetallic compounds (Aoki Group); a study concerning the relationship of the micro-structure, primarily in terms of crystal grain size, of Al_2O_3 and ZrO_2-Al_2O_3-based ceramics to their high-temperature deformation including super-plasticity (Sakuma Group); and a study concerning the preparation of superfine SiC powder by plasma processing, and the sintering characteristics of the powder, for eventual preparation of super-plastic SiC ceramic material (Kijima Group). In addition, a tribological study was conducted for the process of active abrasion/friction in Al_2O_3 due to high-speed sliding (Kato Group).

Fabrication of Nanometer Ceramics Superfine Particles

93FE0111E Tokyo HEISEI SAN NENDO KAGAKU KENKYUHI HOJOKIN in Japanese Mar 92 pp 245-252

[Article by Kazunori Kijima, Department of Engineering, Kyoto Institute of Technology]

[Text]

Fabrication of Nanometer Ceramic Superfine Particles and Super-plastic Ceramics Made from the Particles

1. Introduction

Although super-plasticity can often be observed in metals and eutectic alloys consisting of superfine particles, it is a rare property among ceramics. Silicon carbide ceramics, promising engineering ceramics, have been frequently studied for their strength, although few studies concerning their super-plasticity have been conducted worldwide, and the property has never been found in these ceramics.

Previous studies have indicated that both superfine structure and grain boundary have something to do with super-plasticity. However, it was deemed significant to experimentally confirm if strongly covalent-bonding ceramics with a superfine structure can also be super-plastic regardless of the nature of chemical bonding.

In order to control the particle size of a sintered material to the sub-micron level, we hoped to start a sintering process with a raw material powder with nano-size particles.

In FY90, the characteristics of a powder consisting of superfine particles were determined, and its sintering characteristics were studied. In FY91, the study was continued to try to produce denser silicon carbide ceramics, which were difficult to sinter, with a larger grain size.

A silicon carbide ceramic material with a high purity and a density as high as a theoretical value was successfully obtained. Furthermore, the characteristics of this material were determined.

2. Experiments

Nanometer-size superfine powder of silicon carbide was synthesized by the CVD method using high-frequency inductive coupling-type argon hot plasma. By means of a high frequency transmitter with a transmission frequency of approximately 4 MHz, energy was supplied from a work coil to the plasma-actuating gas through inductive coupling. The plasma furnace made of quartz consisted of three sections; i.e., the gas inlet, plasma transmission and powder precipitation sections.

Details of the synthesis of silicon carbide superfine powder are described in the FY89 report. Argon was used as the plasma-actuating gas, monosilane or silicon tetrachloride was used as the silicon-containing raw material gas, and methane or ethylene was used as the carbon source.

Special care was taken for the synthesis because the powder was superfine. Special attention was paid to the prevention of oxidation and the maintenance of as high a density for the green as possible. The powder was blended with a commercially available powder; the mixture was granulated with a spray dryer and underwent secondary molding by CIP. For sintering, the molded material was hot-pressed in an argon atmosphere.

3. Results

3-1. Sintered Compact of High-Purity, Dense Silicon Carbide

The plasma-synthesized silicon carbide superfine powder was analyzed spark-spectroscopically to find its total cation content, including Fe, Mg and Na ions, to be less than 1,000 ppm. This value indicates the super-high purity of the powder compared with commercially available powders. It appears possible to increase this purity further to that of semiconductors, if a purer raw material gas is used and handled more carefully. The purity of the sintered compact was found to be higher than that of ordinary silicon carbide sintered compacts to such an extent that there was no impurity that affects sintering. Cationic impurities not included in this table [as given], if present, can exist in quantities less than the analytical limits. As clear from the results, it was verified that silicon carbide, even with a high purity, could be sintered under ordinary conditions by manipulating its superfine particles.

The density of the compact ranged from 95% (3.24 g/cm^2) to 100% (3.21 g/cm^2) of the theoretical value, although the density was subject to the raw material powder, blending and hot press conditions.

3-2. Characterization of Sintered Compact

The bending strength of the sintered compact was evaluated with 3 x 4 x 40-mm specimens by the 30-mm span three-point test method. Values of 640 MN/m^2 and 780 MN/m^2 were obtained at room temperature and 1,500°C, respectively. It appears that these strength values could be improved with further experiments and process improvement. The sintered compact showed Vickers hardness values of 23 to 25 GPa, when tested with a diamond indenter under a load of 10 kg/mm^2. These values were greater than ordinary sintered compacts. A fracture toughness value of 4.5 MN/m$^{3/2}$ was obtained for the compact by the IF method. An elastic modulus value of 460 GPa and a Poisson ratio of 0.15 were also obtained for the compact, when tested with the pulse echo method. Although it will be discussed later, this sintered compact seems to be readily processable by discharge fabrication due to its electric conductivity despite the high purity. Thus, this processability will give an advantage to brittle silicon carbide. By the JIS B 0601 test method, a maximum surface roughness (R_{max}) value of 0.03 μm was obtained for a wire-finished surface of the compact, and this fact seems to indicate that this compact can be fabricated even more precisely with further improvement in the sintering process. These mechanical properties are summarized in Table 2.

Table 2. Properties of SiC

Property	Value	Comment
Density	3.2 g/cm^3	Archimedes' method
Strength	640 MN/m^2	(at room temp.)
	780 MN/m^2	(at 1,500°C) 3 points bending test 3 x 4 x 40 mm; span 30 mm
Elastic Modulus	460 GPa	Pulse echo method
Poisson's Ratio	0.15	Pulse echo method
Hardness	25 GPa	Vickers hardness (load: 10 kg/mm^2)
Fracture Toughness	4.6 MN/m$^{3/2}$	Indentation fracture
Thermal Expansion	4.0 x 10^{-6}/°C	(room temp. to 1,000°C)
Thermal Conductivity	210 W/mK	Laser flash method
Specific Heat	0.16 cal/g °C	Laser flash method
Electrical Resistivity	0.01 Ω cm	Four-point probe

Electrical properties, except conductivity, of the sintered compact were not determined. However, it showed a specific resistance value of 10^{-2} Ω x cm in a straight-line region without the varister effect. It is still unclear why the sintered compact is nearly as highly electrically conductive as metals despite its high purity, as indicated in Table 2. In order to clarify the electric conduction mechanism of a highly pure sintered compact, it is necessary to control the purity of the compact, study the sintering process, and compare its superfine structure with a single crystal. Many applications will be open for the ceramic material, if its electric conductivity can be controlled in a broader region, in addition to its high purity and high density.

The laser flash method was used to determine thermal conductivity of the compact which showed a maximum value of 210 W/mK. In this measurement, a specific heat value of 0.16 cal/g x °C was also obtained. The compact was heated to obtain its thermal linear expansion coefficient of 4.0/°C (x 10^{-6}). Therefore, the compact was stable against both heat evolved by the fabrication and thermal shocks.

4. Discussion

4-1. Analysis of Sintering Phenomenon of Silicon Carbide

When a pressed compact of sub-micron-size silicon carbide powder was calcined in an argon atmosphere, grain growth was observed from a temperature near 1,600°C, although structural densification did not take place even at a sintering temperature of 2,000 to 2,300°C. When the sintering process was continued to a higher temperature, the growth of abnormal grains and the recrystallization due to evaporation-aggregation occurred. In other words, the sintered compact's microstructure was not densified, but the texture was porous and coarse due to the presence of the overgrown grains. On the other hand, when a pressed compact of the same sub-micron-size silicon carbide powder with the addition of boron and a phenol resin as sintering aids was calcined in an argon atmosphere, it was observed that the grain growth in the vicinity of 1,600°C was suppressed to a low level, and the structure was densified in a temperature region between 2,000 and 2,300°C.

4-2. Sintering Phenomenon of High-Purity Silicon Carbide

The following three conditions must be met in order to obtain a dense sintered compact of silicon carbide by the solid-phase sintering method.

(1) Driving force for sintering (thermodynamic feasibility).

(2) Rate of sintering (material moving rate theory).

(3) Mechanism of sintering (mechanism).

For a simple filled cube, n = 4, and if its dihedral angle, the driving force for sintering is supposed to exist. According to the dihedral angle measurements by Suzuki and Hase[2] for sintered compact samples of high-purity, no-additive β-SiC powder, approximately 35% of the all samples had the dihedral angles ranging between 99 and 132 degrees, with a peak value of approximately 92 degrees. Greskovich and Rosolowski[3] also obtained similar results for measured dihedral angles, and concluded that the densification should have no problem from the standpoint of energy. These results indicate that no essentially thermodynamic restrictions exist for the densification of silicon carbide.

The activation energy for diffusion is high and the diffusion coefficient is small for silicon carbide, because of its highly covalent nature and great bond strength. The auto-diffusion coefficient of silicon carbide is compared with the same for alumina in Figure 2 [not reproduced]. Due to the high sintering temperatures of 1,900 to 2,300°C, sufficient movement of materials took place in silicon carbide. As discussed above, with both driving force and sintering speed being sufficient for the sintering process of silicon carbide, neither of these conditions should be suspected of undermining the sintering process of silicon carbide.

Let us consider the third condition of sintering mechanism. By Figure 1 [not reproduced] which explains the sintering behavior of silicon carbide, the growth of grains was observed upon heating the high-purity silicon carbide powder, although densification never took place. The growth of grains tells us that the powder system had sufficiently high surface energy to drive the sintering process. In other words, the driving force of the pressed powder of silicon carbide was consumed for grain growth in the initial phase of the sintering process and no energy was left for structure densification. The sintering driving force of silicon carbide was not that great, because sub-micron particles had to be used. Thus, the difficulty of undergoing the sintering process for silicon carbide must be due to its sintering mechanism. The grain growth was promoted by the surface diffusion mechanism in the early stage of the sintering process at a low temperature below 2,000°C. In order to obtain a denser structure for a silicon carbide sintered compact, it is necessary to control the grain growth due to the surface diffusion mechanism, keep the driving force for sintering, and cause material movement from either grain boundaries or within grains to the neck sections through interstitial or volume diffusion at a sintering temperature. Based on this view, it becomes plausible to take the following approaches for obtaining denser sintered silicon carbide.

(1) Use of superfine particulate powder.

(2) Use of sintering aid(s).

(3) Use of new sintering technology.

What was discussed above was the experimental results involving the use of superfine powder.

When superfine particles are used, the driving force for sintering becomes greater, as can be seen from Laplace Equation. Even greater force than what Laplace Equation predicts can be manifested with nano-meter-size superfine particles. There were reports on experiments in which rather poor sintering was experienced with superfine particles. However, the following situations can be surmised for these cases of poor sintering: (1) the particle size was greater than the critical size; (2) the activity of powder was lowered due to contamination of the powder surface by adsorbed oxygen and water due to careless handling of the powder; and (3) the green density was less than 50% TD because of incomplete compacting.

5. Conclusion

A highly pure, dense sintered compact of silicon carbide, which had never previously been prepared, was successfully prepared. After being characterized, this compact was found to have superior physical properties over previous silicon carbide compacts. The particle size of this compact was reduced to less than ⅓ of the previous size, although the size did not quite reach the sub-micron level. The mechanism of grain growth needs to be analyzed, and more experiments need to be run with better grain growth control.

6. References

1. R. L. Coble: "Proc. of 4th Int'l. Conf. on reactivity of Solid," ed. by J. H. Boer.

2. H. Suzuki and T. Hase: "Proc. of Int'l. Symp. of Factors in Densification and sintering of Oxide and Non-oxide Ceramics," (Eds. S. Somiya and S. Saito). Gakujutsu Bunken Fukyukai, p 345 (1978).

3. C. Greskovich and J. H. rosolowski: J. Am. Ceram. Soc. 59, 336 (1976).

4. Shigetoshi Takahashi and Sumio Iijima: Patent Granted (A) 63-8263 (1988).

5. Kazunori Kijima and Mikio Konishi: J. Ceramic Soc. of Japan, 93, 511 (1985).

6. C. M. Hollabaugh, D. E. Hull, L. R. Newkirk and J. J. Petrovic: J. Mater. Sci., 183-190 (1983).

7. Kazunori Kijima: J. Soc. Powder Engineering, 25, 805-811 (1989).

7. Published Dissertations

1. Kazunori Kijima, Makoto Kitamura, Shigeru Akimoto, Toru Uetsuki and Kaichiro Tanaka: "SiC Sintering with Low-Temperature Plasma," J. Ceramic Soc. of Japan, 98 [2].182-186 (1990).

2. K. Kijima: "Sintering of SiC Ultra-Fine Particles," Advanced Materials, 2, 147-156 (1990).

3. Kazunori Kijima: "Ceramics as Advanced Materials," Kogyo Zairyo, 34, 18-20 (1991).

4. Shigeru Akimoto, Kazunori Kijima and Makoto Kitamura: "Change With Time for AlN Densification by Plasma Sintering," J. Ceramic Society of Japan, 100 [2], 196-202 (1992).

5. Shigeru Akimoto, Kazunori Kijima and Eiji Tokuno: "Study Concerning Plasma Sintering Temperature for Y_2O_3-added AlN," J. Ceramic Society of Japan, 100 [5], (1992) (to be published in May 1992).

Books

1. "Ceramic Advanced Materials - Strength and Microstructure - (in part)," Ed. The Ceramic Society of Japan, pp 333-337, Oomu Publishing Co. (1992).

2. "Ceramics Soaring Toward the 21st Century (in part)," Ed. Special Publication Committee, The Ceramic Society of Japan, pp 210-216, The Ceramic Society of Japan (1991).

3. "What Are Ceramics? (in part)" Ed. The Ceramic Society of Japan, p 1, pp 19-20, Oomu Publishing Co. (1991).

4. Video cassette: "Flaming Ceramics I and II (in part)," Ed. Special 100-Year Anniversary Publication Committee, The Ceramic Society of Japan (1991).

5. Kazunori Kijima: "Survey Part I, Production Methods and Applications for Superfine Particles (in part)," pp 228-265 (1991).

8. Oral Presentations

1. S. Akimoto, K. Kijima, T. Uetsuki and K. Tanaka: "Plasma Sintering Behavior of AlN," Abstracts of JSPC-3 p 20 (1990).

2. Kijima, Kitamura, Uetsuki and Tanaka: "Factors Affecting Plasma Sintering of SiC," Draft Paper Collection, Annual Meeting, The Ceramic Society of Japan, p 511 (1990).

3. Akimoto, Kijima, Uetsuki and Tanaka: "Plasma Sintering Behavior of AlN Ceramics," Draft Paper Collection, Annual Meeting, The Ceramic Society of Japan, p 507 (1990).

4. Akimoto, Kijima, Uetsuki and Tanaka: "Effects of Water Adsorbed on AlN Samples on Plasma Sintering," The Fall Symposium, The Ceramic Society of Japan, pp 502-503 (1990).

5. Kijima: "Theory and Examples of Sintering," Basic Discussion Meeting concerning High-Temperature Structural Materials, pp 59-65 (1990).

6. K. Kijima and M. Konishi: "Highly Pure and Fully Densified Silicon Carbide," Abstracts of 92nd Annual Meeting and Exposition, p 377, The American Ceramic Society (1990).

7. Kazunori Kijima: "Densification and Grain Growth," CEPRO, The Ceramic Society of Japan pp 43-63 (1990).

8. Kazunori Kijima, Toru Uetsuki and Kaichiro Tanaka: "Sintering of Silicon Carbide Superfine Powder," The Fall Symposium, The Ceramic Society of Japan, pp 129-130, Basic Discussion Meeting concerning High-Temperature Structural Materials (1990).

9. Kazunori Kijima: "Theory and Examples of Sintering," Ceramics Seminar, pp 59-65 (1990).

10. Kazunori Kijima: "Ceramics Advanced Materials (in part)," pp 333-337, Oomu Publishing Co. (1990).

11. Kazunori Kijima: "Temperature Measurements of Ceramics in Inductively Coupled Plasma; High Temperature Materials; Properties [VII]," p 18 (1991).

12. Kazunori Kijima: "Microstructure of Silicon Carbide After Plasma Sintering," Extended Abstract of 4th International Symposium on Ceramic Materials and Components for Engines, B1, Swedish Ceramic Society, Goteborg, June 10-12 (1991).

13. K. Kijima: "Effects of Gaseous Pressure on Plasma Sintering of SiC," Abstracts of 93rd Annual Meeting and Exposition, p 245, The American Ceramic Society, Cincinnati, 28 April - 2 May 1991 (1991).

14. Akimoto, Kijima, Uetsuki and Tanaka: "Measurement of Plasma Sintering Temperature," Draft Paper Collection, Annual Meeting, The Ceramic Society of Japan, p 417 (1991).

15. Tamaya, Kijima, Uetsuki and Tanaka: "B_2H_6-N_2-Based Plasma CVD Synthesis," Collection of Lectures, Annual Meeting, The Ceramic Society of Japan, p 419 (1991).

16. Yasuhisa Neta, Kazunori Kijima, Toru Uetsuki and Kaichiro Tanaka: "Effects of Sintering Aids in Normal-Pressure Sintering of Silicon Carbide," Collection of Lectures, Annual Meeting, The Ceramic Society of Japan, p 379 (1991).

Strength of Bonded Joint Between Metal and Fiber Reinforced Composite

93FE0111F Tokyo HEISEI SAN NENDO KAGAKU KENKYUHI HOJOKIN in Japanese Mar 92 pp 281-286

[Article by Kozo Ikegami, Precision Engineering Research Institute, Tokyo Institute of Technology]

[Text]

1. Introduction

In order to be practical, a fiber-reinforced composite material must be securely bonded to metallic materials. When a fiber-reinforced composite material is bonded with a metallic material, the effects of the shape and condition of the joint on its strength needed to be clarified. In this study, attempts were made to examine how the shape of the joint affected its initial breakage strength, when a tensile load was applied to the single lap, scarf or shaft bonded joint between a carbon fiber-reinforced material (CFRP) and a piece of carbon steel or stainless steel.

2. Method

2-1. Joint Model

The shapes of the three different joint models are shown in Figure 1. These joints were formed by bonding the sides of a metal plate and a laminated plate made of a fiber-reinforced material, the two beveled ends of these same plates, and a stepped metal shaft and a cylindrical sleeve made of a fiber-reinforced material. A carbon steel was used for the metallic part to form the lap and scarf joints, whereas both carbon steel and stainless steel were used for the metallic part to form shaft joints. The fiber-reinforced material for these joints were made by molding carbon fiber fabrics into a plate and a cylinder with the fibers properly oriented. Epoxy resin was used for bonding.

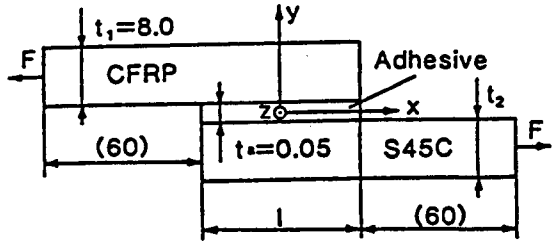

t_2=6.0,8.0,18 l=8.0,20,40,60,80
w=25 σc=F/t_1w
$\bar{L}$=l/t_1 $\bar{T}$=t_2/t_1 $\bar{X}$=x/l

（ａ）重ね合わせ接合

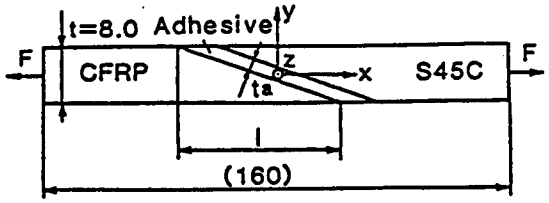

ta=0.05 l=16,24,32,40,60,80
w=25 $\bar{L}$=l/t σc=F/t_1w

（ｂ）きりそぎ接合

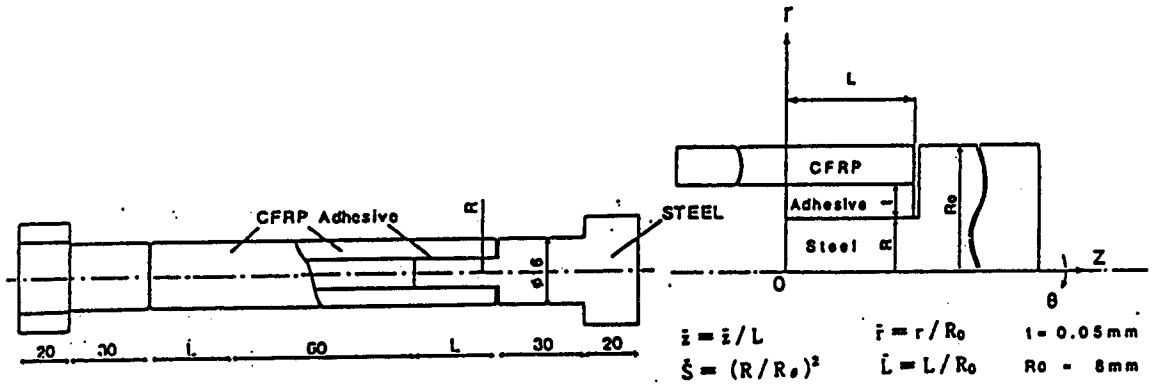

(1)接合部の拡大図

（ｃ）円筒軸接合

Figure 1. Joint Models

Key: (a) Single lap joint; (b) Scarf joint; (c) Shaft joint; (1) Expanded diagram of shaft joint

2-2. Strength Evaluation

Stress analysis was conducted for the joints under a tensile load. The rules of strength for the particular joint-component materials were applied to the results of the analysis, in order to evaluate the strength of the joints. In other words, a joint was tested for its strength as follows. The stress distribution throughout the joint was first analyzed by the finite element method. The joint was then divided into four parts, i.e., CFRP, metal, adhesive layer and bonding interface. For each part, the rule of strength of its particular material was applied to the stress distribution within that part. More specifically, a tolerable load for each of the CFRP, metal, adhesive layer and bonding interface parts, was calculated by using the rule of strength with the stress distribution in each part, and the initial breakage strength of the joint was determined from the minimum tolerable load value. (Hoffman's) rule [1] was used as the rule of strength for the CFRP, (Meeses)' rule was used for the metal and the adhesive layer, and the bonding strength rule [2] was used for the interface between the metal and the adhesive layer.

3. Results

Joint strengths, in terms of the lap length ratio, are shown in Figures 2 through 5 for the single lap, scarf and shaft joints. Each curve in these graphs indicates the initial breakage stress value calculated from the stress distribution for each bonded material, the adhesive or the bonded interface by applying the corresponding rule of strength. The smallest value in all of these curves in each graph is the initial breakage strength for that particular joint. The white and black circles in the graphs respectively indicate experimentally obtained values for the stress causing initial breakage in a joint and for the stress causing the joint to break apart.

In Figure 2, the relationship of the tensile strength to the lap length is shown for the bonded single lap joint between a CFRP and carbon steel. The graph indicates that the breakage stress at the bonded interface is smaller than the others, i.e., the strength of the interface governs the joint's strength. It also indicates that the joint strength increases with the increasing lap length.

In Figure 3, the relationship of the tensile strength to the lap length is shown for the bonded scarf joint between a CFRP and carbon steel. Similar to the graph in Figure 2, this graph also indicates that the breakage stress at the interface is the smallest and it determines the strength of the entire joint. With the increase in the lap length, the strength of the joint first decreases slightly before showing an increasing trend.

In each of Figures 4 and 5, the relationship of the tensile strength of the shaft joint to the lap length is shown, with the metal part being carbon steel for the case in Figure 4, and stainless steel for the case in Figure 5. In the case of the bonded joint with carbon steel, the break stress at the interface determines the joint strength. However, in the case of stainless steel,

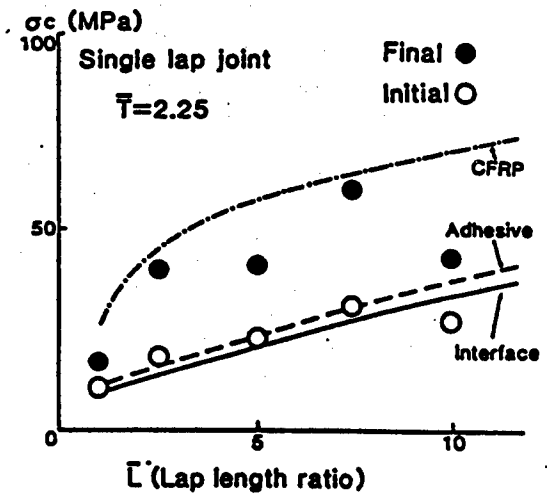

Figure 2. Tensile Strength of Single Lap Joint

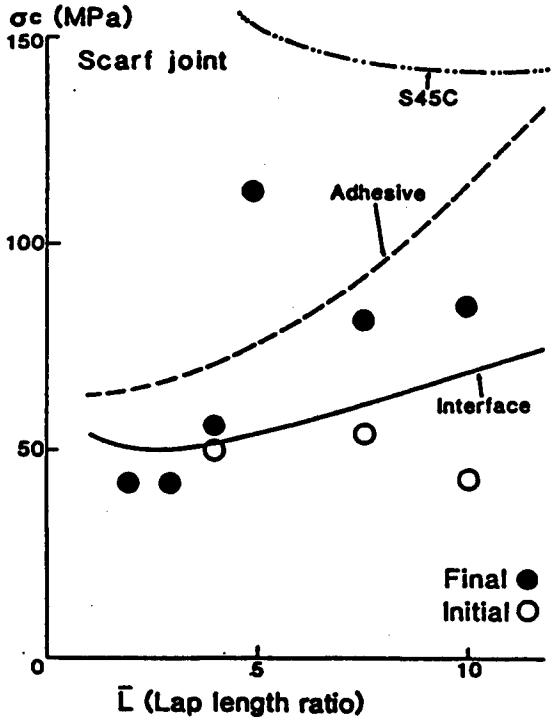

Figure 3. Tensile Strength of Scarf Joint

the break stress at the interface varies with the lap length. Thus, when the lap length is short, the joint strength is governed by the break stress in the CFRP part, whereas the break stress at the interface determines the joint strength for greater lap lengths. For either metal, the bonded joint strength becomes saturated with the increasing lap length, so that the joint strength remains the same after the lap length exceeds a certain value.

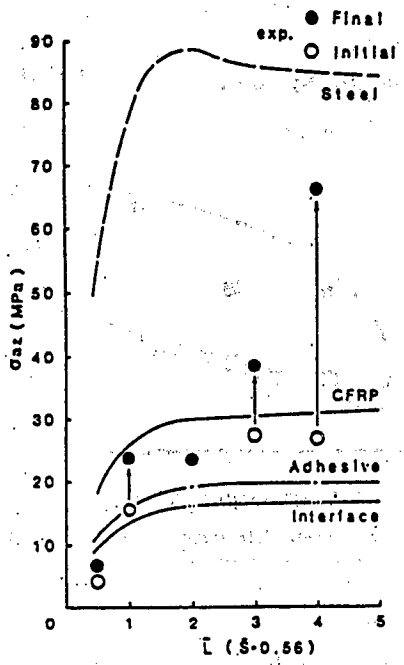

Figure 4. Tensile Strength of Shaft Joint (with Carbon Steel Shaft)

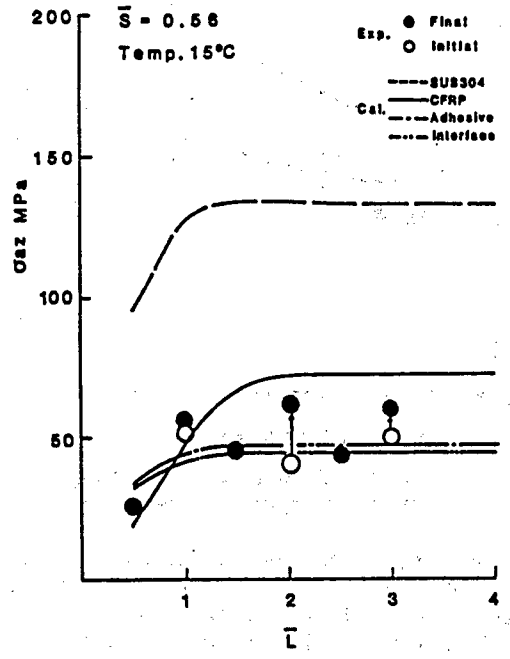

Figure 5. Tensile Strength of Shaft Joint (with Stainless Steel Shaft)

4. Discussion

In comparing the actual strengths for the single-lap and scarf joints for a given lap length, as shown in Figures 2 and 3, when the lap length is short, the scarf joint is stronger than the single-lap joint. The reason is that stresses are less concentrated at the tip of the bonded area in the scarf joint than in the single-lap joint. On the other hand, for longer lap lengths, the scarf joint strength becomes weaker than the single-lap joint. The reason for this is that, a break is initiated in the scarf joint, which has a longer lap length, when transverse-direction fibers in the CFRP plate, which is the adherend, are pulled off by a stress smaller than the break strength of the plate.

Between the two shaft joint cases with different metallic materials, as shown in Figures 4 and 5, the bonded joint with the stainless steel shaft shows a higher initial break strength than the bonded joint with the carbon steel shaft. However, the latter shows a greater load stress increase from the initial break through the final bond rupture. At any rate, in either case, breaks always occurred nearly at the interface, and there was no significant difference in elastic properties between carbon steel and stainless steel. Based on these facts, the nature of the interface appears to have affected the joint strength in each of the shaft joints.

5. Conclusion

A CFRP and a metallic material were bonded in three ways; single-lap, scarf and shaft. The bonded joints' strengths were examined. The stress distribution in the bonded area under a tensile load was analyzed by the finite element method for each bonded joint. The initial break strength of each bonded joint was determined from the smallest value among the calculated tolerable load values for each component part of the joint, i.e., CFRP, metal, adhesive layer and interface, from the stress distribution and the appropriate strength rule. These calculated values were checked against experimental values. Based on these results, the relationship of the bonded CFRP-metal joint form to the joint strength was clarified.

6. References

1. Tai, Sugibayashi and Ikegami: Dissertations Part A, The Japan Society of Mechanical Engineers, 53 (1987) p 491, 1426.

2. Ikegami: Dissertations Part A, The Japan Society of Mechanical Engineers, 50 (1984) p 457, 1557.

7. Published Papers

1. Funatsu, Sato and Ikegami: "Strength of Bonded Joint of Metal Shaft in CFPR Sleeve," Journal of the Adhesion Society of Japan, 28 (1992) pp 50-56.

2. Sato and Ikegami: "Tensile Strength of Bonded Joint of Stainless Steel Shaft in CFRP Sleeve at Low Temperature," Journal of the Japan Society of Mechanical Engineers, Part A (in press).

8. Oral Presentation

1. K. Ikegami and T. Sugibayashi: "Strength of Shaft Joint with Adhesive Coupling," Proceedings of XIX Congress A.F.T.P.V. (1991) pp 305-308.

Composition and Strength of Ceramic Composite Materials

93FE0111G Tokyo HEISEI SAN NENDO KAGAKU KENKYUHI HOJOKIN in Japanese Mar 92 pp 421-428

[Article by Toshio Hirai and Mamoru Omori, Metal Research Institute, Tohoku University]

[Text]

1. Introduction

Previously we reported that the compound $Y_4Al_2O_9$ appeared to transform into martensite [1]. With the exception of long fiber-reinforced composite materials, this martensite transformation has been considered to be the most effective tool to cause toughness improvement in ceramics [2]. Today, zirconia is the only practically utilized martensite transformation ceramic compound. Zirconia undergoes the martensite transformation at a temperature higher than 1,000°C. Initially, zirconia research was primarily concerned with a study of the toughness improvement phenomenon due to stress-induced phase transition in a temperature region between the martensite transformation temperature and the reverse martensite transformation temperature. However, since it was recently reported that super-elastic phenomena appeared in zirconia above the reverse martensite transformation temperature, new opportunities have been envisioned for zirconia [3, 4]. Shape-memory alloys have been prepared based on the martensite transformation, and the alloys have been in the limelight as a new functional metallic material. Similar functional materials could be developed from zirconia, and these new materials should include not only superbly tough zirconia, but also eventually shape-memory ceramics. If compounds other than zirconia that undergo the martensite transformation can be used for ceramics, the functions of ceramics should certainly be drastically broadened with manifestation of the above-mentioned function in many areas.

Nine rare earth elements, Sm through Lu, were reported to form compounds with the same composition and crystal structure as those of $Y_4Al_2O_9$. The idea was to study the structures of these 10 compounds, and attempt to synthesize many highly tough, super-elastic ceramics through transformation control in the same manner as done to zirconia. Another idea was, by taking advantage of the fact that these compounds, unlike zirconia, can be made into sintered compacts with SiC or Si_3N_4 under normal pressure, to synthesize many sintered compacts and composite materials with the silicon compounds, in which strength, toughness and hardness were altered. Discussed in this report are our confirmation of the martensite transformation of the compounds, results of our experiments for controlling the transformation, and composite materials between these compounds and SiC.

2. Methods

Raw materials for synthesizing $Y_4Al_2O_9$-based compounds were rare earth oxides (Y_2O_3 and Ho_2O_3, 99.9% pure, made by Nippon Yttrium Co., Ltd.) and Al_2O_3 (99.99% pure, made by Asahi Chemical Industry Co., Ltd.). The raw materials were blended for 72 hours in a ball mill by a wet method with alcohol. After alcohol was evaporated, the blended powder was added to a 5% polyethylene glycol aqueous solution, and the mixture was mixed well before dried. This dried powder was packed in a metal cast for uniaxial molding under a pressure of 10 MPa and for CIP molding under a pressure of 100 MPa with a hydrostatic press. This green compact was heated in air to 500°C at a rate of 2°C/min, and maintained at 500°C for two hours to remove polyethylene glycol. The compact was then heated to 1,600 to 1,920°C at a rate of 8°C/min, and kept at a specified final temperature for a specified time to produce a sintered compact. For the synthesis of composites, SiC (0.3 μm, made by Ibiden Co., Ltd.) was added to $Y_4Al_2O_9$ and Al_2O_3, and the similar methods were used to produce greens and remove polyethylene glycol.

Subsequently, the composite greens were heated in a nitrogen atmosphere to 1,825°C at a rate of 50°C/min, and maintained at this temperature for 10 minutes. The crystalline structures of the sintered materials were examined with an x-ray diffraction device (RAD-B, made by Rigaku Denki K.K.), and the micro-structures were observed with an electron microscope (2000 EX, made by JEOL Ltd.). The three-point bending test method with a cross-head speed of 0.005 cm/min, a span of 20 mm, and an Autograph (DSS-500, made by Shimadzu Corp.) was used to determine hardness of samples. An ultra-high temperature thermomechanical analyzer (1,700°C TMC, made by Rigaku Denki K.K.) was used to check thermal expansion characteristics of the materials with a heating rate of 10°C/min, using an atmosphere of air for simple sintered compacts and an atmosphere of an inert gas for composite compacts. The indentation method with a load of 98N was used to determine fracture toughness values. Measurements of Vickers hardness at room temperature were made with a Vickers hardness tester (MVK-E, made by Akashi Co., Ltd.), while hardness measurements at high temperatures were made with a high-temperature hardness tester (QM, made by Nippon Kogaku K.K. (Nikon)).

3. Results

3-1. $Y_4Al_2O_9$ Sintered Compacts

An x-ray diffraction graph for $Y_4Al_2O_9$, which was synthesized from 2 Y_2O_3 and Al_2O_3, is shown in Figure 1. The graph indicates the presence of a slight residue of Y_2O_3, although no diffraction peaks due to Al_2O_3 can be seen. Shown in Figure 2 [as given] is the thermal expansion of this sintered compact as a function of temperature. The reverse martensite transformation appears to start at 1,390°C and complete at 1,430°C, while the martensite transformation begins at 1,370°C and ends at 1,330°C.

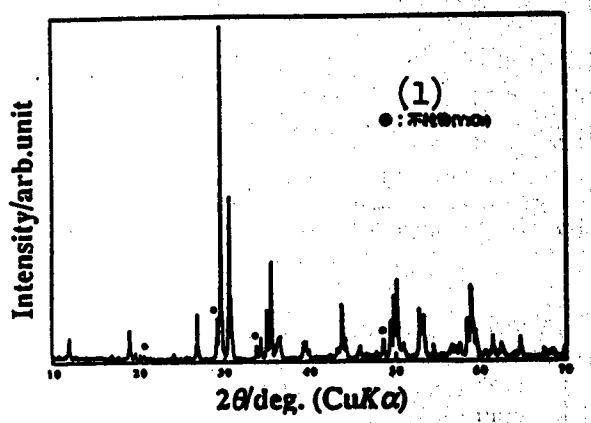

Figure 1. X-Ray Diffraction Diagram for $Y_4Al_2O_9$ Sintered Compact (1,920°C)

Key: 1. Impurity (Y_2O_3)

Attempts were made to control the transformation of $Y_4Al_2O_9$ by adding different oxides, and SiO_2 was found to be most effective. Thus, sintered compacts were prepared by adding a quantity ranging 0.5 to 4 weight percent of SiO_2 to $Y_4Al_2O_9$. The relationship of Vickers hardness value of the compact to the sintering temperature is illustrated in Figure 2. The graph shows clearly that the hardness increases, therefore, the density increases, with the sintering temperature. Since the curves in the Figure 2 graph could be divided into two groups, the 1% addition and the 3% addition of SiO_2 were selected to represent each of the two groups in all subsequent experiments. The relationships of the densities of the compacts with 1 and 3% of SiO_2 added to the sintering temperature are shown in Figure 3.

Although the theoretical density of $Y_4Al_2O_9$ is reportedly 4.518 g/cm^3[5], the density of the compact with 3% SiO_2 exceeds this value at a sintering temperature of 1,750°C or higher. For the same two compacts with 1 and 3% SiO_2 and sintered at two different temperatures of 1,750°C and 1,800°C, thermal expansion values were measured at various temperatures. These are shown in Figures 4 and 5, respectively. A volume change appears to take place due to the transformation in the vicinity of 1,400°C for the compact with 1% SiO_2, although no volume change appears for the compact with 3% SiO_2. However, the compact with 3% SiO_2, sintered at 1,800°C seems to undergo volume change due to new transformation in the vicinity of 500°C. When observed with a transmission electron microscope, the compact with 1% SiO_2 formed twin crystals. However, the twin crystal formation disappears when the SiO_2 addition quantity is increased from 1 to 3%. The greatest strength value was recorded to be 148 MPa for the compact with 1% SiO_2, sintered at 1,750°C, although the highest toughness value was 3.7 MPam$^{1/2}$ for the compact with 1% SiO_2, sintered at 1,800°C.

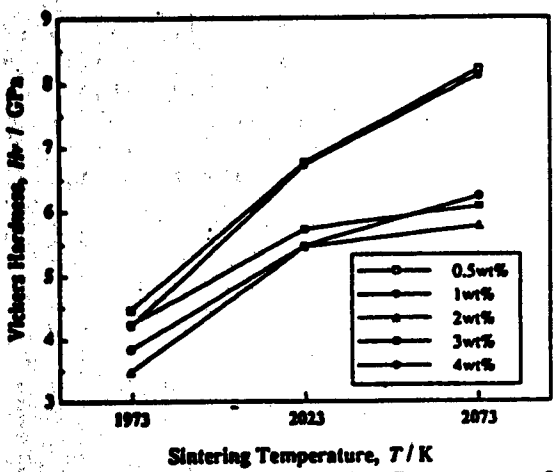

Figure 2. Relationship of Sintering Temperature of $Y_4Al_2O_9$ to Its Vickers Hardness

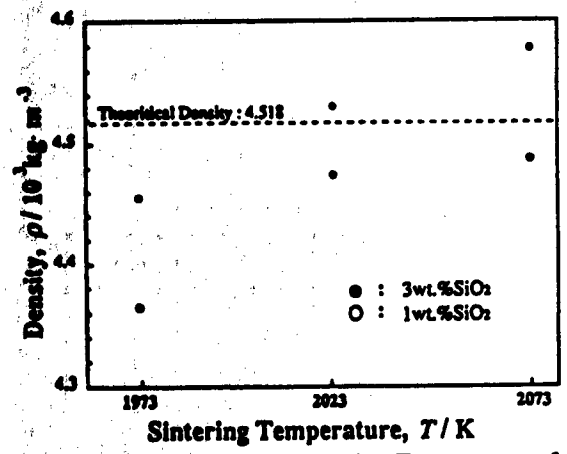

Figure 3. Relationship of Sintering Temperature of $Y_4Al_2O_9$ to Its Density

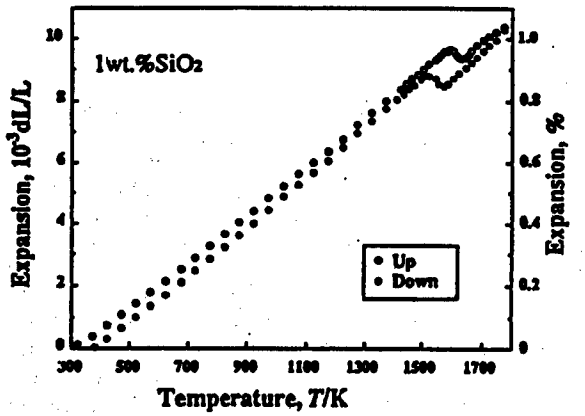

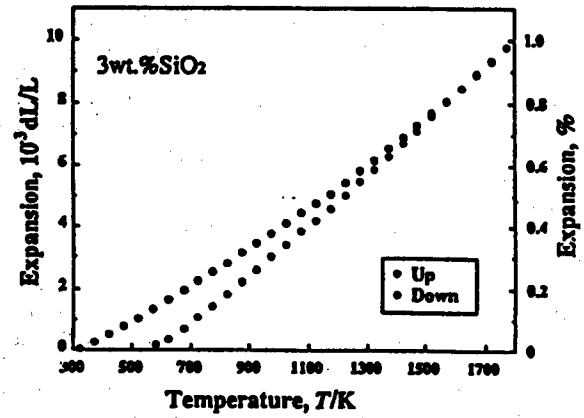

Figure 4. Thermal Expansion Curves for 1,750°C-Sintered $Y_4Al_2O_9$ Compacts

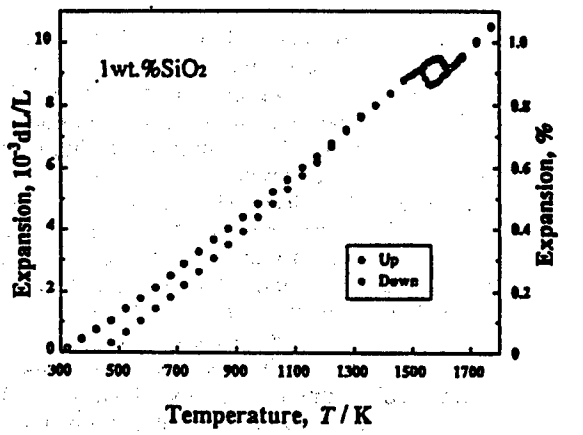

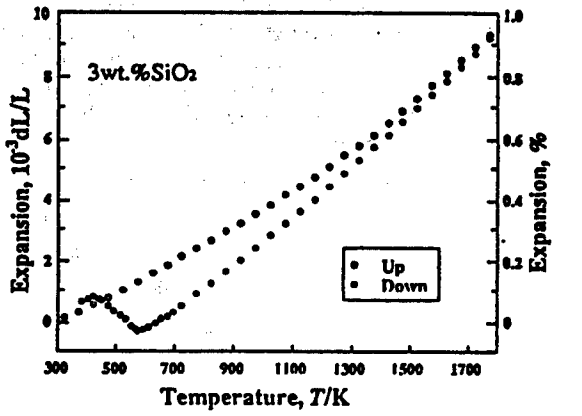

Figure 5. Thermal Expansion Curves for 1,800°C-Sintered $Y_4Al_2O_9$ Compacts

3-2. $Ho_4Al_2O_9$ Sintered Compacts

An x-ray diffraction graph for a sintered compact of $Ho_4Al_2O_9$ synthesized at 1,650°C is shown in Figure 6. The graph indicates the presence of residual Ho_2O_3, one of the raw materials. Shown in Figure 7 is the thermal expansion of a sample sintered at 1,600°C as a function of temperature.

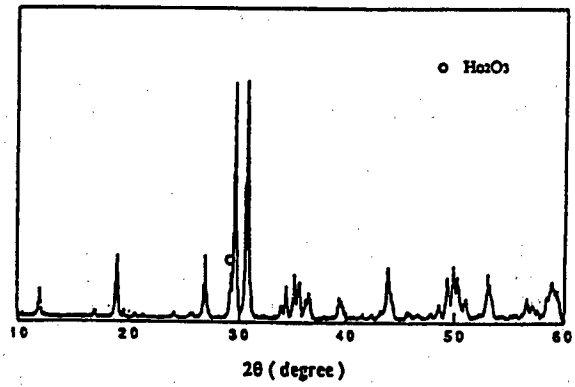

Figure 6. X-ray Diffraction Graph for $Ho_4Al_2O_9$ Sintered (1,650°C)Compact

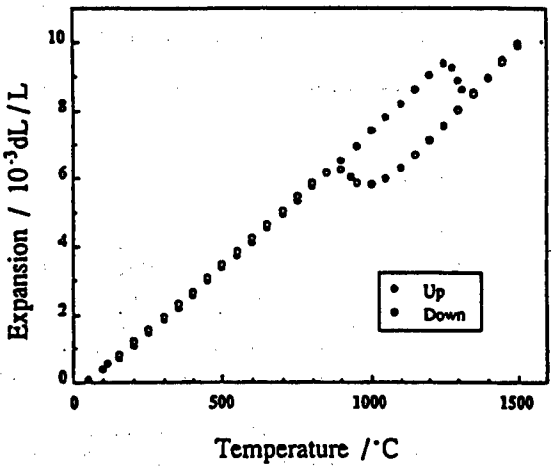

Figure 7. Thermal Expansion Curves for $Ho_4Al_2O_9$ Sintered (1,600°C) Compact

The thermal expansion curves show a volume change due to the martensite transformation above 1,000°C. A transmission electron micrograph of this particular sample is shown in Figure 8 [photo not reproduced]. Although larger grains of this sample have diameters more than 10 μm, no twin crystal formation due to the transformation can be observed, but strain figures appear instead. Therefore, the volume change in this compact due to the transformation is alleviated by the crystalline deformation without twin crystal formation. Similar thermal expansion curves are plotted against temperature for a 1,600°C-sintered sample of $Ho_4Al_2O_9$ containing 0.5% SiO_2 which was added. A volume change is noticeable from the curves which show no hysteresis. The amount of volume change did not change due to the addition of SiO_2. Another compact sintered at 1,650°C gave bending strength and fracture toughness values of 155 MPa and 3 $MPam^{1/2}$, respectively. With the increase in the amount of SiO_2 added, the compact tended to be more porous and less dense, although the grain size became smaller.

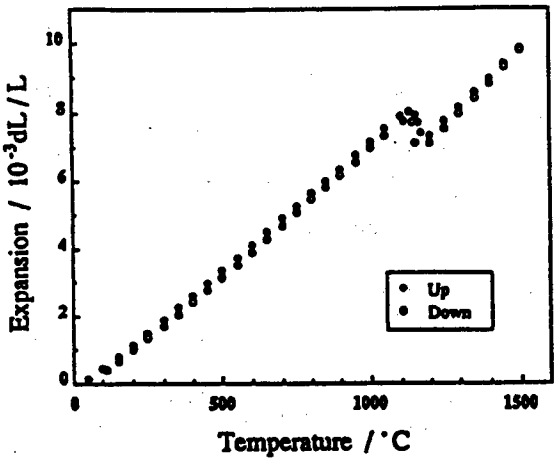

Figure 9. Thermal Expansion Curves for Sintered (1,600°C) Compact of $Ho_4Al_2O_9$ With 0.5% SiO_2 Added

3-3. SiC-$Y_4Al_2O_9$ (SiO_2)

It was learned that the transformation of $Y_4Al_2O_9$ could be controlled by the addition of SiO_2. Thus, a composite material was synthesized from 50-weight-percent SiC and 50-weight-percent $Y_4Al_2O_9$ (containing 3-weight-percent SiO_2) by sintering at 1,830°C for 10 minutes. This composite was found to be dense and thoroughly sintered. Thermal expansion of this composite was measured against temperature, and there was no volume change as was for $Y_4Al_2O_9$ containing 3% SiO_2. Transmission electron microscopic observation did not detect the formation of twin crystals due to the transformation. The composite showed a bending strength value of 430 MPa.

4. Discussion

It was clarified that the compound $Y_4Al_2O_9$ would undergo the martensite transformation accompanied by volume change at a high temperature of 1,330°C. The magnitude of volume change due to this transformation amounted to approximately one third of that for zirconia. The transformation of zirconia is from monoclinic to tetragonal. Although the crystalline structure of the compound $Y_4Al_2O_9$ at low temperatures is reportedly monoclinic [5], we are currently analyzing the same structure at high temperatures in the absence of any published data. In order to control the transformation, similar to the case of zirconia, various oxides were added to $Y_4Al_2O_9$ to prepare sintered compacts for examination. Among the oxides, SiO_2 was found to be most effective. When the added amount of SiO_2 was increased from 0.5 to 4 weight percent, the volume change phenomenon ceased to appear after the amount of SiO_2 exceeded 3 weight percent, although a new volume change occurred at a lower temperature when the sintering temperature was raised to 1,800°C. This fact agrees well with the observation that, when MgO was added to zirconia, the typical volume change disappeared and a new one appeared at a lower temperature after a heat treatment [6]. Nevertheless, the sintered compact of $Y_4Al_2O_9$ containing SiO_2 showed low toughness and strength values, indicating no effect of transformation control upon toughness improvement. The following two facts may explain this. First, the particle sizes were over 10 μm, and secondly, the sintered compact of $Y_4Al_2O_9$ contained residual Y_2O_3, the raw material, as shown in Figure 1. This is because the composition of this compound is non-stoichiometric, and the raw material will remain as an impurity in a stoichiometric blend. It is conjectured that the presence of high-density Y_2O_3 caused the density of the sintered compact of $Y_4Al_2O_9$ containing 3% SiO_2 to exceed the theoretical density value. Currently, attempts are being made to control the particle size, and optimize the composition.

As shown in Figure 7, the sintered compact of $Ho_4Al_2O_9$ also underwent the martensite transformation at a temperature above 1,000°C. The transformation of this compound also changed with the addition of SiO_2.

Therefore, it appears also possible to control the transformation. The sintered compact of this compound showed a low bending strength value and an insignificant toughness value. As shown in Figure 8, strains due to the volume change caused by the transformation existed in this compact. The strains are believed to have weakened both strength and toughness. The addition of SiO_2 did not produce a denser compact, although it diminished the particle size. Therefore, perhaps with further efforts, a dense compact with appreciable strength and toughness may be obtained. The raw material, Ho_2O_3, also remained in the sintered compact of $Ho_4Al_2O_9$, and its composition is likely to be non-stoichiometric.

The composite material, SiC-$Y_4Al_2O_9$ (3% SiO_2), could be synthesized by sintering under normal pressure.

There were no twin crystals in its oxide matrix. The sintered material showed thermal expansion curves without a volume change and with controlled transformation. The material's strength was at the practical level, although not as great as anticipated, probably because the matrix was not sufficiently toughened.

5. Conclusions

1. The compound, $Y_4Al_2O_9$, undergoes the martensite transformation at temperatures above 1,330°C.

2. The martensite transformation of $Y_4Al_2O_9$ can be controlled by the addition of SiO_2.

3. The compound, $Ho_4Al_2O_9$, also undergoes the martensite transformation at temperatures above 1,000°C, and the transformation can also be controlled by the addition of SiO_2.

4. The composite material, SiC-$Y_4Al_2O_9$ (3% SiO_2), can be obtained by sintering under normal pressure.

5. Neither strength nor toughness of the sintered compacts and the composite material was high. It appears necessary to reduce particle sizes and optimize compositions with the elimination of impurities.

References:

1. M. Omori, A. Sakuma and T. Hirai: "Ceramics Today - Tomorrow's Ceramics," Edited by P. Vincenzini, Elsevier Sci. Publ. (1991) pp 1327-1335.

2. A. G. Evans: J. Am. Ceram. Soc. 73 [2], 187-206 (1990).

3. A. V. Virkar and R. L. K. Matsumoto: J. Am. Ceram. Soc. 69 [10], C224-226 (1986).

4. P. E. Reyes-Morel, J. S. Cherng and I. W. Chen: J. Am. Ceram. Soc. 71 [8], 648-657 (1988).

5. J. W. Reed and A. B. Chase: Acta Cryst. 15 812-813 (1962).

6. M. V. Swain: Nature 322, 234-235 (1986).

Published Dissertations:

1. M. Omori, Z. Chen, T. Koide and T. Hirai: "$Ho_4Al_2O_9$ Polycrystal Ceramics," First International Symposium on Science of Engineering Ceramics, Edited by S., Kimura and K. Niihara, The Ceramic Society of Japan (1991) pp 515-520.

2. M. Omori, K. C. Hsu, S. Tsunekawa and T. Hirai: "Thermal and Dielectric Properties of Zirconyl Phosphate Compact," J. Mat. Sci. 27 [2], 408-412 (1992).

3. M. Omori, A. Sakuma and T. Hirai: "Role of Alumina in the SiC-Y_2O_3-Al_2O_3 System," (in press) Proceedings of MRS Japan (1992).

4. M. Omori, T. Koide and T. Hirai: "$Yb_4Al_2O_9$ Composite Material," Powder and Powder Metallurgy 39 [6] (1992) (in press).

Oral Presentations:

1. M. Omori, A. Sakuma and T. Hirai: "Synthesis of SiC-Y_2O_3-Al_2O_3 Composite Material and Its Properties," Spring Symposium, Japan Institute of Metals, 2-4 April 1991.

2. M. Omori, A. Sakuma, T. Koide, T. Hirai and K. Nishiyama: "Synthesis of SiC-Ln_2O_3-Al_2O_3 Composite Material and Its Properties," Symposium, Annual Meeting, The Ceramics Society of Japan, 22-24 May 1991.

3. M. Omori, Z. Chen, T. Koide and T. Hirai: "Synthesis of $Ho_4Al_2O_9$ Polycrystal Ceramics," Fall Symposium, Japan Institute of Metals, 1-3 October 1991.

4. M. Omori, Z. Chen, T. Koide and T. Hirai: "Synthesis of SiC-$Yb_4Al_2O_9$ Composite Material," 4th Fall Symposium, The Ceramics Society of Japan, 15-18 October.

5. M. Omori, T. Koide and T. Hirai: "SiC-$Yb_4Al_2O_9$ Composite Material," Fall Symposium, Japan Society of Powder and Powder Metallurgy, 26-28 November.

6. T. Koide, M. Omori and T. Hirai: "Syntheses of $Y_4Al_2O_9$ and SiC-$Y_4Al_2O_9$ Ceramics and Their Properties," Research Forum, Tohoku-Hokkaido Section Meeting, The Ceramics Society of Japan, 7-8 November 1991.

7. T. Koide, M. Omori and T. Hirai: "Synthesis of Ln_2O_3-Al_2O_3-SiC Composite Ceramic Material and Its Properties," 30th Discussion Meeting on Ceramics Basic Science, 23-24 January 1992.